D-to-A_{eff} converter

Speaker/Author: Patrick Egan

Company: National Institute of Standards and Technology

100 Bureau Dr, Gaithersburg, MD 20899

egan@nist.gov

Co-Authors: Eric Stanfield and John Stoup

Abstract:

Recent developments in diameter metrology at NIST have enabled the dimensional characterization of piston-cylinder assemblies (PCA) with unprecedented precision. For the newest generation of PCA, standard uncertainty on measurement of outer diameter is 12 nm, while uncertainty on measurement of inner diameter is 14 nm. With a high-accuracy dimensional dataset in hand, the task of determining the pressure generated by a specific PCA is reduced to converting diameter (and straightness and roundness) to effective area (and distortion coefficient).

Details on how this was done for the artifact PCA2062 are described. PCA2062 was dimensioned in 2017 and 2020; the area repeated within $0.2 \times 10^{-6} \cdot A_{\text{eff}}$. The calculation produced estimates of fall-rate and rotation-decay that agree with experimental observations within 12 %. Fall-rate is proportional to the square of gap-width, so the agreement between calculation and measurement validates the dimensional estimate of gap-width within (36 ± 42) nm, where the 42 nm uncertainty is governed by the present state of flow theory. Finally, an estimate of uncertainty in the effective area of a dimensioned artifact is provided: as expected, diameter is the main culprit, but there are open questions with the flow model that preclude an accurate evaluation of the distortion coefficient. For the 530 kPa operating range of PCA2062, distortion is not a significant problem, but the effect would be dominant in assemblies operating 1 MPa and above.

1 Introduction and motivation

An experimental effort is underway to measure the refractivity of helium gas at the level of $10^{-6} \cdot (n-1)$. The motivation is that a precision measurement of helium refractivity at known temperature allows a realization of the pascal, in what is sometimes called the optical pressure scale [1]. The underlying principle is the ideal gas law, which defines pressure $p = \rho R T$ in terms of molar density ρ and temperature T; the gas constant R is a fixed value. The interest in helium (refractivity) is because the Lorentz–Lorenz equation provides a direct link between refractivity and density $\rho = \frac{2}{3A_R}(n-1) + \cdots$ via the polarizability A_R. Polarizability is a fundamental property of a single atom, and for helium, it can be calculated [2] well-within $10^{-6} \cdot A_R$. Consequently, the realization $p = \frac{2}{3A_R}(n-1)RT$ provides a well-understood physical system, in which all input parameters are known without reference to an ancillary measurement of pressure. The ultimate accuracy of this new scale can approach the $u(T)$-limit; or, how well the thermodynamic temperature of the helium gas can be known.

One attraction [3] of the optical pressure scale is that it neither relies on artifacts nor restricted materials. Indeed, one stimulant to perfecting the optical realization is that it

has potential to settle the twenty-five-year old, unresolved disagreements in mechanical pressure scales—unresolved disagreements which have been at the level of $5 \times 10^{-6} \cdot p$ for piston gages [4], and $15 \times 10^{-6} \cdot p$ for mercury manometers [5]. To meaningfully conclude on past disagreements requires that one can compare a new optical realization to a traditional mechanical realization at the highest levels of accuracy. It is this necessity for a best-effort realization of the mechanical pressure scale that motivates the present work. At the National Metrology Institute (NMI) level, the outlook [3] is that the optical pressure scale will supersede the mechanical scale in terms of accuracy, reliability, and universality.

Towards this best-effort realization of the mechanical pressure scale, three sets of piston-cylinder assemblies (PCA) have been dimensioned, and their effective areas established traceable to the SI meter. These state-of-the-art PCA comprise a 50 mm-diameter fixed piston with a floating/rotating cylinder. The PCA2062 was manufactured in 2014, coarse dimensioned in 2015, fully dimensionally-characterized in 2017, and redimensioned in 2020 [6]. Next follows some details on how these dimensional datasets were converted to effective area, which rely heavily on two references by Sabuga and coworkers [7, 8]. The procedure begins by fusing together three separate dimensional inputs (diameter, straightness, and roundness) to form a birdcage model of the artifact. Then, the pressure-induced distortion is added to the birdcage; the distortion is calculated by finite-element methods, and needs one parameterized input, which is the pressure distributed down the gap between the piston and cylinder. This distributed pressure is calculated based on the theory of rarefied gas dynamics. Finally, the cross-sectional area of the distorted birdcage is calculated. The following explanation will attempt to logically work backwards: starting from the output (area), and unwinding step-by-step to the input (dimensions).

2   Calculation procedure

The pressure generated by the piston-gage is given by

$$p_{\mathrm{pg}} = \frac{mg}{A_{\mathrm{eff}} \left[1 + (t_{90} - 20) \cdot 2\alpha_{\mathrm{WC}} \right] \cdot (1 + b)} + p_{\mathrm{vac}}, \tag{1}$$

where m is a mass load and g is local gravity. The effective area A_{eff} is described more below, and is estimated chiefly by dimensional measurements made at $t_{90} = 20\ {}^\circ\mathrm{C}$; when the piston-gage operates away from this reference temperature, its diameter (effective area) must be scaled for the thermal expansion α_{WC}. (The notation t_{90} refers to temperature measurement on the international temperature scale of 1990.) As pressure inside the cylinder increases, the piston and cylinder deform, thus changing the diameter (effective area); the deformation parameter b accounts for pressure-induced distortion. Finally, Eq. (1) must balance for pressure acting outside the cylinder; in the present case, operation is in "absolute mode" and the pressure outside the cylinder p_{vac} is pumped to < 0.3 Pa, and measured with a capacitance diaphragm gage.

The effective area A_{eff} of the PCA must take into account forces caused by flow and friction in the gap—the space between the piston and cylinder, which is approximately 580 nm. Historically, these forces were estimated by the theory of Dadson [9], which assumed viscous flow. The more recent theory of Sharipov [7, 10] is based on rarefied gas dynamics, which computes a flow coefficient determined by the level of rarefaction for all pressures and dimensions distributed down the gap. For a pressure differential across the

gap $p_1 - p_2$ (in this case $p_2 = p_{\text{vac}}$), Sabuga, Sharipov, and Priruenrom [7] write the area at pressure $A_0 = A_1 - A_2 - A_3$ having three components [11]

$$A_1 = \frac{\pi \mathcal{G}_{\text{c1}}^2 p_1 - \pi \mathcal{G}_{\text{c2}}^2 p_2}{p_1 - p_2}$$

$$A_2 = -\frac{\pi \int_0^{l_{\text{c}}} h_z \cdot \mathcal{G}_{\text{c}} \frac{\mathrm{d}p_z}{\mathrm{d}z} \mathrm{d}z}{p_1 - p_2} \tag{2}$$

$$A_3 = -\frac{2\pi \int_0^{l_{\text{c}}} p_z \cdot \mathcal{G}_{\text{c}} \frac{\mathrm{d}\mathcal{G}_{\text{c}}}{\mathrm{d}z} \mathrm{d}z}{p_1 - p_2}.$$

The effective area A_{eff} is found by calculating A_0 for several different p_1, and extrapolating $p_1 \to 0$; the distortion coefficient b is deduced from the slope of the extrapolation. In A_0, the first component A_1 is the area upon which the mass-force acts, and depends on the radius (generatrix) at top $\mathcal{G}_{\text{c1}}$ and bottom $\mathcal{G}_{\text{c2}}$ of the cylinder. The generatrix of a cylinder, described below, is obtained as the line that minimizes deviations between three sets of dimensional measurements: straightness, roundness, and point-to-point diameter. The other two components in (2) are A_2 and A_3, and arise from the drag forces owing to gas flow in the gap and surface curvature; both of these components require knowledge of the pressure distribution p_z along the gap, and need the gap dimensions to be updated for pressure-induced distortion. The width of the gap $h_z = \mathcal{G}_{\text{c}} - \mathcal{G}_{\text{p}}$ is the difference between the generatrixes of cylinder and piston. The height of the cylinder $l_{\text{c}} = 40$ mm includes a 2 mm extrapolation of diameter measurements at both ends of the cylinder. The coordinate system is shown in Fig. 2(a); z is along the cylinder axis and x is radial; the variables $\mathcal{G}_{\text{c,p}}$, h_z, and p_z are all functions of z.

The calculation is iterative [12]: First there is a calculation of the pressure distribution from p_1 down to p_2 along the gap

$$p_z = p_1 + (p_2 - p_1) \frac{\int_0^z [h_z \cdot G_{\text{P}}]^{-1} \mathrm{d}z}{\int_0^{l_{\text{c}}} [h_z \cdot G_{\text{P}}]^{-1} \mathrm{d}z}, \tag{3}$$

which requires the Poiseuille coefficient [10, 13]

$$G_{\text{P}} = a_{00} + \begin{cases} \frac{1}{2\sqrt{\pi}} \ln \frac{\mathcal{G}_{\text{c}}}{h} + \frac{\pi}{2} & \text{for } \delta \leq 4 \times 10^{-4} \\ \sum_i a_i \cdot \log(\delta)^i & \text{for } \delta > 4 \times 10^{-4}, \end{cases} \tag{4}$$

the interpolation of which is based on evaluation of the rarefaction parameter [10, 13]

$$\delta_z = \frac{p_z h_z}{\eta v_{\text{mp}}} \tag{5}$$

where η is gas viscosity, and $v_{\text{mp}} = (2RT/M)^{1/2}$ is the most probable speed and depends on the gas constant R, temperature T, and molar mass M. For G_{P} at $\delta > 4 \times 10^{-4}$, a 12th-order polynomial is fit to the solution [10] of the one-dimensional, infinite plate, planar Poiseuille flow, with coefficients a_i

$$a_0 = 1.547801 \qquad a_1 = -7.215365 \times 10^{-3} \qquad a_2 = 1.270563 \times 10^{-1}$$
$$a_3 = 2.027864 \times 10^{-2} \qquad a_4 = 3.679723 \times 10^{-3} \qquad a_5 = 1.707451 \times 10^{-3}$$
$$a_6 = 5.697987 \times 10^{-4} \qquad a_7 = 6.654191 \times 10^{-5} \qquad a_8 = -7.441006 \times 10^{-6}$$
$$a_9 = -2.983074 \times 10^{-6} \qquad a_{10} = -3.433585 \times 10^{-7} \qquad a_{11} = -1.806107 \times 10^{-8}$$
$$a_{12} = -3.699704 \times 10^{-10}.$$

A numerical algorithm to calculate G_{P} is given in Ref. [10]. The function of (4) is plotted in Fig. 1(a), together with output from the algorithm of Ref. [10]; the function (4) is modified from Ref. [10] as follows. The two-part function of (4) is clipped [7] as
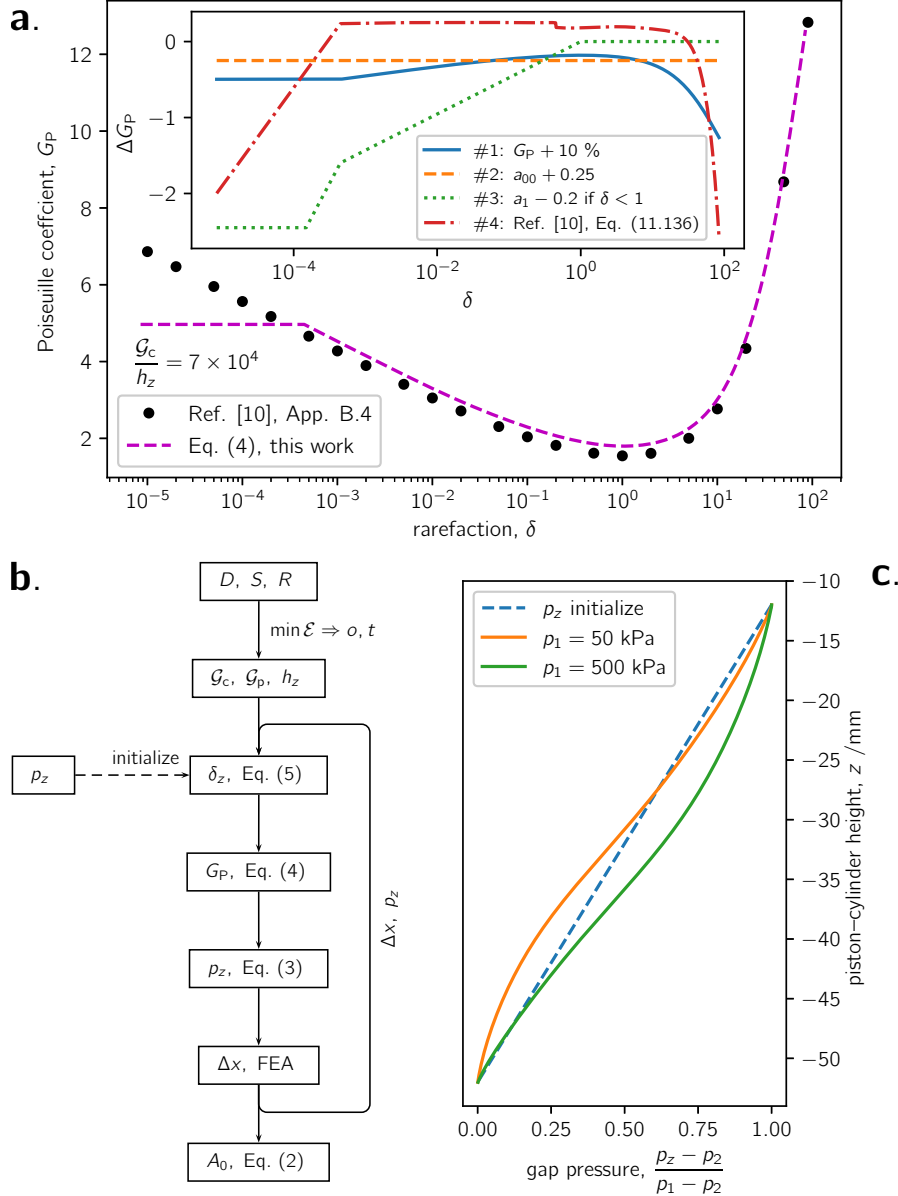
Figure 1: (a.) Poiseuille flow coefficient derived from Ref. [10] and modified to the physical situation of the present work. The inset figure shows the difference between (4) and four error cases covering $u(G_{\mathrm{P}})$. (b.) Block diagram of the procedure to calculate A_0. (c.) Pressure distribution down the gap p_z for two cases in helium, $p_1 = 50$ kPa and $p_1 = 500$ kPa, and with $p_2 = 0$.

$\delta < 4 \times 10^{-4}$ to approximate the annular flow [14] in the limit $\frac{\mathcal{G}_P}{\mathcal{G}_c} \to 1$; this patch addresses the problem with the infinite plate solution, in which G_P tends toward infinity as $\delta \to 0$. The clipping threshold is specific to each PCA geometry [7] by the quotient $\frac{\mathcal{G}_c}{h_z}$; it is worth noting that for PCA2062, even at helium pressures as low as $p_1 = 10$ kPa (and $p_2 = 0$), the annular flow approximation applies to less than 2 % of the gap region, and its influence on A_0 is negligible. The function (4) allows for a tangential momentum accommodation coefficient of 0.9, by setting the offset factor $a_{00} = 0.25$. Lack of knowledge about the accommodation coefficient is a main contributor to uncertainty in the theory of rarefied
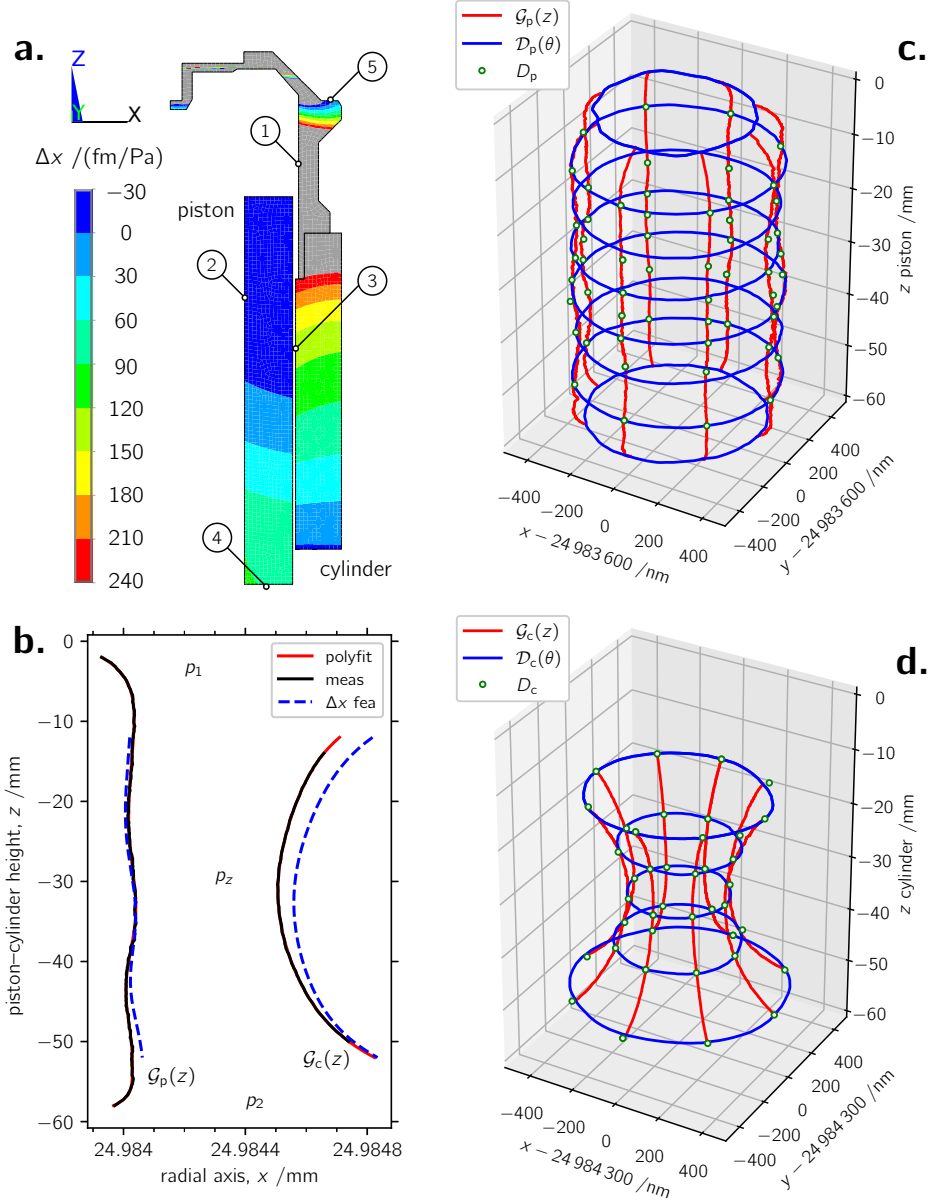
Figure 2: (a.) Finite-element model of pressure-induced distortion in the piston and cylinder. (b.) Least-squares-adjusted generatrixes of piston and cylinder, with overlay of pressure-induced distortion at $p_1 = 500$ kPa and $p_2 = 0$. (c. and d.) "Birdcage" model of piston and cylinder constructed by fusing three sets of dimensional data: straightness, roundness, and point-to-point diameter.

gas dynamics; the four perturbations to G_{P}, plotted in the inset of Fig. 1(a), are also relevant to the uncertainty.

In the calculation of p_z, the terms p_z and δ_z are interdependent, and so iteration is required for convergence. (To startup, δ_z is initialized with a linear distribution of pressure down the gap.) The procedure must also be iterated for h_z, because the width of the gap changes, caused by pressure-induced distortion of the piston and cylinder. The pressure-induced distortion is computed using finite-element analysis (FEA), which is parameterized for the pressure load p_z applied to the gap, obtained by calculation of (3). This all works with a master Python script which handles several things: (i) calculates p_z based on the most recent estimate of G_{P} and h_z; (ii) dynamically updates two FEA scripts (one piston script and one cylinder) with p_z and runs the FEA program; (iii) extracts/imports Δx from the FEA displacement results along the PCA engagement region; (iv) updates $\mathcal{G}_{\mathrm{p}}$ and $\mathcal{G}_{\mathrm{c}}$ for the respective Δx, recomputing p_z and G_{P}; and (v) iterates. An overview block diagram of the calculation procedure is shown in Fig. 1(b). The computed area converges within $10^{-8} \cdot A_{\mathrm{eff}}$ after two iterations [see Fig. 3(a)], and the main advantage of this "closed-loop" implementation is that numerical investigation of model sensitivity to input errors can be performed with versatility. Another closed-loop benefit is demonstrated in Fig. 3(c): the effective area and distortion coefficient can be calculated throughout the cylinder fall down the piston—something impractical to do with an open-loop implementation which hand-transcribes settings from one program to another. The FEA is shown in Fig. 2(a), which is actually two separate simulations of piston and cylinder, which have been clipped to the same Δx colorscale and combined (the width of the gap is arbitrarily exaggerated in x). The FEA model is axisymmetric about $x = 0$, and the boundary conditions are also annotated in Fig. 2(a): ① pressure p_1 applied to partial inner surface of cylinder, ② pressure p_1 applied to inner, top, partial outer, and partial bottom surface of piston, ③ distributed (gap) pressure p_z applied to engaged segments of piston and cylinder as a function of z, ④ piston constrained in z (by clamped o-ring), ⑤ lip of cylinder constrained in z (by mass load). The distorted profiles of the piston outer diameter and cylinder inner diameter, along the region of engagement, are extracted from the FEA and added to the generatrix (actual dimensional measurements) in Fig. 2(b), with $p_1 = 500$ kPa. Fig. 2(b) is also annotated with the locations of the pressure "regions" p_1, p_z, and p_2.

The dimensional inputs to (2) are the generatrixes of piston and cylinder. Dimensional characterization provided high-density data traces of roundness and straightness, and low-density data on point-to-point diameter. The best estimate of the artifact geometry is obtained by fusing together (synchronizing [8]) the intersecting points in the three sets of measurements. In Ref. [8], the generatrix and directrix

$$
\begin{aligned}
\mathcal{G}(z) &= S_\theta(z) + o + t \cdot z \\
\mathcal{D}(\theta) &= R_z(\theta) + q + w \cos\theta + v \sin\theta
\end{aligned}
\tag{6}
$$

are found by adjusting the measured straightness $S_\theta(z)$ and roundness $R_z(\theta)$ by the model parameters o, t, q, w, v. Straightness $S_\theta(z)$ is a function of height z, and is indexed for each trace made in azimuth θ; the parameters offset o and taper t are vectors of dimension equal to the number of traces in θ (which is 8 for both piston and cylinder). Roundness $R_z(\theta)$ is a function of θ, and is indexed for each trace made in z; the parameters q, w, and v are vectors of dimension equal to the number of traces in z (which is eight for the piston and five for the cylinder). The model parameters are deduced by least-squares

minimization of the objective function

$$\mathcal{E}^2 = \min_{o,t,q,w,v} \sum_{i=1}^{5} \left(\frac{\sum e_i^2}{N_i} \right), \tag{7}$$

which has

$$
\begin{aligned}
e_1 &= \mathcal{G} - \mathcal{D} \\
e_2 &= \frac{D - (\mathcal{G} + \mathcal{G}')}{2} \\
e_3 &= \frac{D - (\mathcal{D} + \mathcal{D}')}{2} \\
e_4 &= \frac{D_{\text{ref}}}{2} - \mathcal{G}_{\text{ref}} \\
e_5 &= \frac{D_{\text{ref}}}{2} - \mathcal{D}_{\text{ref}},
\end{aligned}
\tag{8}
$$
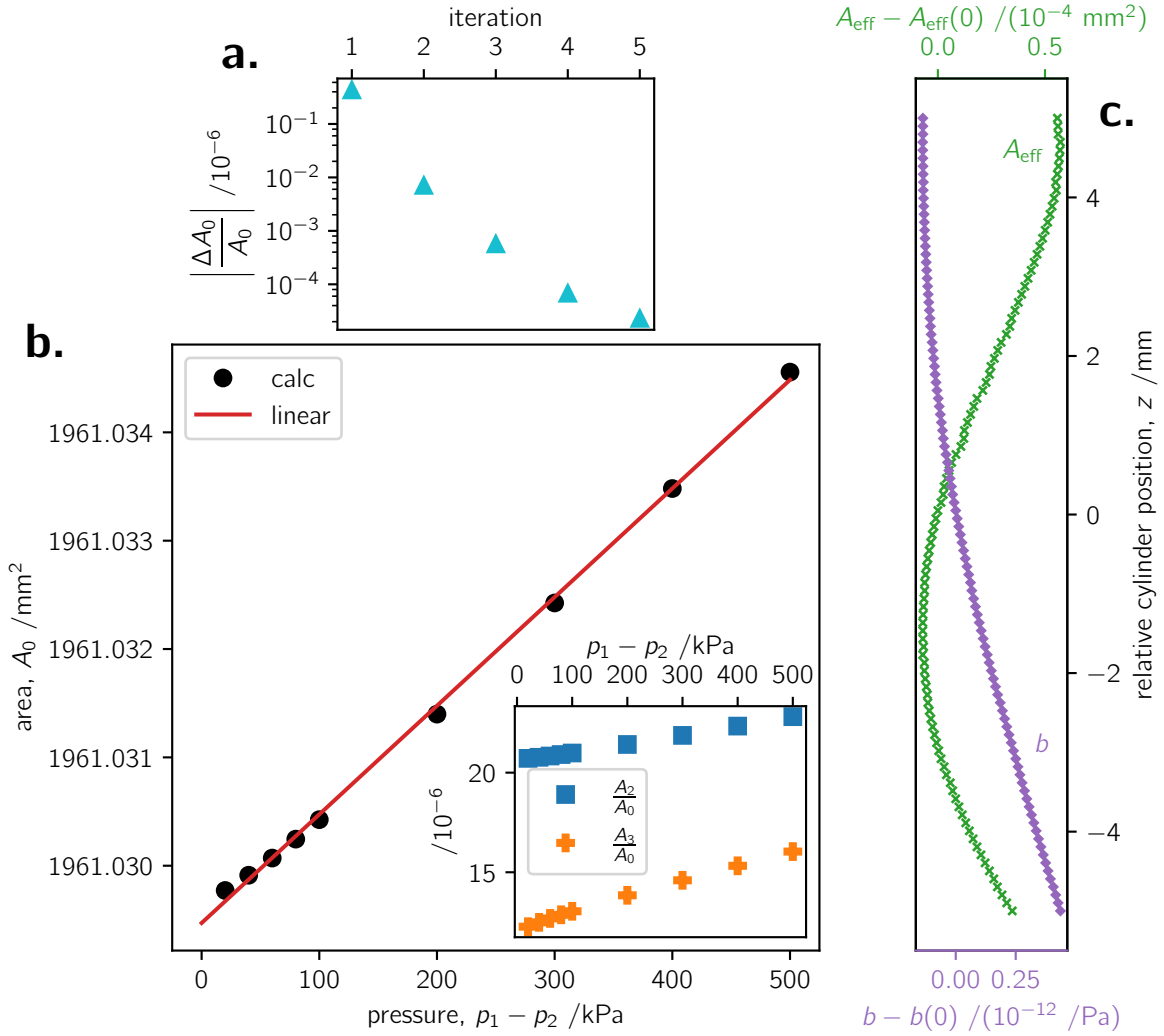
Figure 3: (a.) Convergence of the p_z and FEA iteration loop. (b.) Calculated area as a function of pressure for the piston–cylinder assembly PCA2062 in "absolute mode" with $p_2 = 0$. Inset: relative contributions of A_2 and A_3 to A_0. (c.) Change in A_{eff} and b, relative to values at $z = 0$, as the cylinder falls down the piston.

and D are the measured point-to-point diameters. (The term $\mathcal{E}$ is the root-mean-square error of the optimization, and is a metric of statistical uncertainty. The integer N_i is the sample size of each residual error matrix e_i.) The flow calculation of Sabuga, Sharipov, and Priruenrom [7] uses the generatrix $\mathcal{G}$ of the piston and cylinder to calculate the cross-sectional area that best describes a three-dimensional artifact. The residual matrices e_4 and e_5 in (8) are setup as reference points to define the coordinate system in which the dimensional adjustment is performed. This means they are setup as sparse matrices of four diameters; two at different z heights and two at different θ azimuthal angles; the choice of height and angle is arbitrary. The notation $\mathcal{G}'$ and $\mathcal{D}'$ refers to the generatrix and directrix at the opposite azimuthal orientation.

The least-squares adjusted datasets are shown in Fig. 2(c) and (d); these plots are sometimes called the "birdcage" [15, 16]. The plot of the piston in Fig. 2(c) has been scaled in the radial axis by subtracting 49.9672 mm from the diameter; the plot of the cylinder in Fig. 2(d) has had 49.9686 mm subtracted from the diameter. Once the vectors o and t have been found by the least-squares adjustment of the intersecting points, each straightness trace can be converted to its respective $\mathcal{G}$. The result is a set of eight $\mathcal{G}$ which are a function of z, and are indexed for each straightness trace in θ. For calculation of A_0, the eight $\mathcal{G}$ are averaged over θ.

Finally, this dimensional characterization of $\mathcal{G}$ is used in the area calculation of (2), to produce a determination of $A_0 = A_1 - A_2 - A_3$ as a function of pressure. The A_0 result is plotted in Fig. 3(b); the relative contributions of A_2 and A_3 are shown in the inset of Fig. 3(b). From this, the effective area of PCA2062 has been determined

$$A_{\text{eff}}^{2062} = 1961.0292(37) \cdot \left[1 + 5.06(73) \times 10^{-12} \cdot \frac{p}{\text{Pa}}\right] \ \text{mm}^2$$

in helium at 20 °C, and valid for the dimensional characterization of 2020. The distortion coefficient b is best described by a linear term. The estimation from the slope of the line in Fig. 3(b) is for a monolithic assembly. The final estimate given above is 3.8 % smaller than the slope of the line in Fig. 3(b); this reduction in distortion is based on a finite-element simulation of a 0.1 mm epoxy joint between the titanium (cap) and tungsten carbide that forms the hollow cylinder assembly.

The uncertainty budget for this determination is listed in Table 1, and will be described elsewhere. Here is briefly mentioned that dimensional measurements comprise the chief contributor, among which the entry "instability" refers to reproducibility of the PCA2062 in the dimensionings of 2017 and 2020. A history and control chart may reduce this uncertainty component over the coming decades. The largest contributor to flow is the entry "$\mathcal{G}$" which represents standard deviation among the 64 pair-selections of piston and cylinder generatrixes. On this point it is emphasized that the boundary conditions of the flow model have fixed walls (Poiseuille flow), which does not describe the rotating cylinder.

3 Conclusion

A procedure has been described to convert a dimensional dataset to effective area for a specific PCA. The procedure first fuses together all dimensional inputs (diameter, straightness, and roundness) to form the birdcage and average generatrix. The flow (distributed pressure) down the gap between piston and cylinder is then calculated using the theory of rarefied gas dynamics. Next, the distributed pressure is parameterized to load

Table 1: Standard uncertainty in mechanical pressure generated by PCA2062.

component	$u(p_{\mathrm{pg}}) \times 10^6$
A_{eff}	
dimensional	1.7
D, 13 nm	
$\mathcal{E}$, 9.9 nm	
extrapolation, 10 nm	
α_{WC}, 4.6 nm	
compression, 3 nm	
instability, 17.8 nm	
flow	0.7
RGD, 2.9×10^{-4} mm^2	
$\mathcal{G}$, 13×10^{-4} mm^2	
h_z, 0.1×10^{-4} mm^2	
b	0.4
m	54 mPa + 0.1
g	0.2
p_{vac}	25 mPa
combined ($k = 1$)	$[(60 \text{ mPa})^2 + (1.9 \text{ μPa/Pa})^2]^{1/2}$

a finite-element model, which estimates geometric distortion to the generatrixes. Finally, the calculation is iterated to convergence. The entire procedure runs in a self-contained Python script, which executes the finite-element program as a function call.

Based on the quality of the dimensional characterization, its reproducibility, and a detailed error analysis, it seems realistic that the artifact PCA2062 can approach 2 μPa/Pa standard uncertainty. It is pointed out that the authoritative work of Schmidt *et al.* [16] claimed $3.0 \times 10^{-6} \cdot p$ uncertainty on the 36 mm diameter PCA39, which, when scaled for differences in diameter, would translate to $2.2 \times 10^{-6} \cdot p$ for the 50 mm diameter PCA2062—despite a generation of progress in dimensional metrology and flow modeling, the performance of the (other) last artifact-based standard [3] remains essentially unchanged. Indeed, if anything, the checkered history of piston gage claims [4, 17], together with recent evidence in key comparisons of diameter [18, 19], urge caution below the 5 μPa/Pa level (125 nm in diameter). Crossfloat comparisons that show agreement between force and diameter ratios at fractionally within 10^{-6} may lead to false-confidence: ratios validate consistency of the dimensional characterization, not its accuracy. What is needed is a stringent test between the optical and mechanical pressure scales at the level of a few $10^{-6} \cdot p$.

References

[1] K. Jousten, "A unit for nothing," Nature Physics **15**, 618 (2019).

[2] M. Puchalski, K. Piszczatowski, J. Komasa, B. Jeziorski, and K. Szalewicz, "Theoretical determination of the polarizability dispersion and the refractive index of helium," Physical Review A **93**, 032515 (2016).

[3] W. D. Phillips, "The end of artefacts," Nature Physics **15**, 518 (2019).

[4] G. F. Molinar, B. Rebaglia, A. Sacconi, J. C. Legras, G. P. Vailleau, J. W. Schmidt, J. R. Stoup, D. R. Flack, W. Sabuga, and O. Jusko, "CCM key comparison in the pressure range 0.05 MPa to 1 MPa (gas medium, gauge mode). Phase A1: Dimensional measurements and calculation of effective area," Metrologia **36**, 657 (1999).

[5] M. Perkin, R. Köhler, P. Riety, T. Skrovanek, E. C. Morris, C. R. Tilford, C. D. Ehrlich, A. Ooiwa, G. Eichorn, J. Jäger, G. F. Molinar, A. H. Bass, and A. C. Gupta, "Comparison of pressure standards in the range 10 kPa to 140 kPa," Metrologia **35**, 161 (1998).

[6] J. Stoup, W. Ren, E. Stanfield, and P. Egan, "Piston-sleeve diameter characterization at NIST," In preparation for Metrologia.

[7] W. Sabuga, F. Sharipov, and T. Priruenrom, "Determination of the effective area of piston–cylinder assemblies using a rarefied gas flow model," in *PTB-Mitteilungen*, Proceedings of the 5th CCM International Conference on Pressure and Vacuum Metrology, Vol. 121, edited by K. Jousten (Physikalisch-Technische Bundesanstalt, 2011) pp. 260–262.

[8] W. Sabuga and T. Priruenrom, "An approach to the evaluation of dimensional measurements on pressure-measuring piston-cylinder assemblies," in *Proceedings of the Joint International Conference IMEKO TC3/TC16/TC22* (2007).

[9] R. S. Dadson, S. L. Lewis, and G. N. Peggs, *The pressure balance: theory and practice* (Her Majesty's Stationery Office, London, 1982).

[10] F. Sharipov, *Rarefied Gas Dynamics: Fundamentals for Research and Practice* (Wiley-VCH, Weinheim, Germany, 2016) Chap. 11 & App. B.

[11] R. S. Dadson, R. G. P. Greig, and A. Horner, "Developments in the accurate measurement of high pressures," Metrologia **1**, 55 (1965).

[12] A. H. Bass, "Analysis of mechanical pressure generators," Journal of Physics E: Scientific Instruments **11**, 682 (1978).

[13] F. Sharipov, "Application of the Cercignani–Lampis scattering kernel to calculations of rarefied gas flows. I. plane flow between two parallel plates," European Journal of Mechanics B/Fluids **21**, 113 (2002).

[14] S. S. Lo, S. K. Loyalka, and T. S. Storvick, "Rarefied gas flow in a cylindrical annulus," Journal of Vacuum Science & Technology A **1**, 1539 (1983).

[15] K. Jain, W. Bowers, and J. W. Schmidt, "A primary dead-weight tester for pressures (0.05–1.0) MPa," Journal of Research of the National Institute of Standards and Technology **108**, 135 (2003).

[16] J. W. Schmidt, K. Jain, A. P. Miiller, W. J. Bowers, and D. A. Olson, "Primary pressure standards based on dimensionally characterized piston/cylinder assemblies," Metrologia **43**, 53 (2006).

[17] P. L. M. Heydemann and B. E. Welch, *Experimental Thermodynamics Volume II*, edited by B. Le Neindre and B. Vodar (Springer US, Boston, MA, 1968) Chap. 4, Part 3: Piston Gages, pp. 147–202.

[18] G. B. Picotto, "Final report on EUROMET.L-K4: Calibration of diameter standards, group 1," Metrologia **47**, 04003 (2010).

[19] E. Bánréti, "Final report on EUROMET.L-K4: Calibration of diameter standards, group 2," Metrologia **47**, 04001 (2010).